Available online at www.sciencedirect.com
ScienceDirect
Journal of the European Ceramic Society 29 (2009) 1963–1970
www.elsevier.com/locate/jeurceramsoc

Increase of Mn solubility with decreasing grain size in ZnO

Boris Straumal [a,b,*], Brigitte Baretzky [a], Andrei Mazilkin [b], Svetlana Protasova [b], Ata Myatiev [c], Petr Straumal [c,d]

[a] *Max-Planck-Institut für Metallforschung, Stuttgart, Germany*
[b] *Institute of Solid State Physics, Russian Academy of Sciences, Chernogolovka, Russia*
[c] *Moscow Institute of Steel and Alloys (Technological University), Moscow, Russia*
[d] *Institut für Materialphysik, Universität Münster, Münster, Germany*

Received 15 August 2008; received in revised form 13 December 2008; accepted 7 January 2009
Available online 1 February 2009

Abstract

Nanograined (grain size 20 nm) ZnO films with various Mn content (from 0 to 47 at%) were synthesized by the novel wet chemistry method. The solubility limit for Mn was determined at 550 °C. The lattice parameter c of the ZnO-based solid solution with wurzite structure ceases to grow at 30 at% Mn. The peaks of the second phase (Mn_3O_4 with cubic lattice) become visible in the X-rays diffraction spectra at 30 at% Mn. The same second phase appears in the bulk ZnO already at 12 at% Mn. The recently published papers on the structure and magnetic behaviour of Mn-doped ZnO allowed us to obtain the size-dependence of Mn solubility in ZnO for the polycrystals and small single-crystalline particles. The overall Mn solubility drastically increases with decreasing grain size. The quantitative estimation leads to the conclusion that, close to the bulk solubility limit, the thickness of an Mn-enriched layer is several monolayers in GBs and at least two monolayers in the free surfaces.

Keywords: Grain size; Grain boundaries; Impurities; Surfaces; ZnO

1. Introduction

The phase diagrams for the nanograined materials can drastically differ from those for the single crystals or coarse-grained polycrystals. For example, by increasing the content of an alloying component, c, a solubility limit is reached at a certain concentration, c_s. Above c_s the second phase appears in the bulk. By further increasing c, only the amount of the second phase increases, but the concentration in the first phase remains equal to c_s. The easiest way to measure c_s is to follow the change of the lattice spacing in the solid solution, for example with the help of X-rays diffraction (XRD). The lattice spacing continuously changes with increasing c up to c_s. At $c > c_s$ the lattice spacing remains unchanged, and the diffraction peaks of a second phase appear in the XRD spectrum.

However, if the alloy contains surfaces and interfaces with segregated second components, the total concentration of a second component, c_t, will be higher than the concentration in the bulk solid solution, c_v. The difference between c_t and c_v would increase with an increasing specific area of surfaces and interfaces (i.e. with decreasing grain size). If the grain size is small enough, the difference between c_t and c_v can become measurable. This is due to the fact that XRD registers the diffraction only from the bulk phases. The component segregated in the thin surface or interface layers remains invisible for XRD. The XRD peaks appear only in the case where the coherent-scattering region is large enough (grain size around 5 nm or larger). Simultaneously, XRD allows one to measure the grain size using the angle dependence of the peak width.

McLean was probably the first who mentioned that the apparent solubility limit, c_{sa}, in the fine grained materials will be higher than the volume solubility limit c_s.[1] He calculated this difference for the Fe–C system and grain size of 1 μm and 10 μm.[1] Beke et al. calculated the shift of miscibility gap due to the GB segregation in dependence on number of GB layers.[2,3] Experimentaly such shift was observed in the Pd–H system.[4] The increase of the total solubility with decreasing grain size was observed for Ti and Y in alumina[5,6] and for Y and Ca in TiO_2.[7,8] Nevertheless, the consistent XRD measurements of

* Corresponding author.
E-mail addresses: straumal@mf.mpg.de, straumal@issp.ac.ru (B. Straumal).

0955-2219/$ – see front matter © 2009 Elsevier Ltd. All rights reserved.
doi:10.1016/j.jeurceramsoc.2009.01.005

solubility shift c_{sa}–c_s in dependence on grain size d are very time-consuming and, to the best of our knowledge, were never conducted before. Zinc oxide offers a good possibility for such successive investigation. ZnO is broadly used as a transparent conducting oxide in the semiconductor thin film technology, as a material for varistors (doped by Bi_2O_3) and for gas sensors. Moreover, it is a promising material for future spintronics as a possible ferromagnetic semiconductor. Ferromagnetic semiconductors could allow seamless electrical manipulations of magnetic states and magnetic modification of electric signals. In 2000 Dietl et al. theoretically predicted that ZnO doped by small amounts of "magnetic" impurities like Mn or Co should possess the ferromagnetic properties.[9] This work triggered a boom of experimental work. In the meantime more than 1200 papers devoted to dilute magnetic semiconductors have been published. Unfortunately, ferromagnetism in diluted doped ZnO is far from understood. The presence or absence of ferromagnetism in doped ZnO critically depends on the synthesis method. Fortunately, these studies allow the dependence of c_{sa}–c_s on the grain (particle) size d to be estimated.

Therefore, the goal of this work is threefold, (1) to measure the solubility shift c_{sa}–c_s in nanograined ZnO manufactured by the novel wet chemistry method; (2) to analyse the c_{sa}–c_s dependence on the grain size in the broad interval of d using the published data on ZnO; (3) to compare the influence of segregation in surfaces and interfaces (i.e. grain boundaries, GBs) on the shift c_{sa}–c_s at the same grain (particle) size d.

2. Experimental procedure

The Mn-doped ZnO thin films were deposited on the Al foils by the novel wet chemistry method. The substrates were dip-coated by the mixture of liquid organic acids with metallic ions and dried at 150 °C. Then the deposited layers were oxidized in air at 550 °C. The resulting films were greenish and transparent. The film thickness was determined by electron-probe microanalysis (EPMA) and edge-on transmission electron microscopy (TEM) and measured between 50 and 200 nm. The Mn content in films was between 0 and 47 at%. The zinc and manganese contents in doped oxides were measured by atomic absorption spectroscopy in a PerkinElmer spectrometer and by EPMA in a Tescan Vega TS5130 MM microscope equipped by the Oxford Instruments LINK energy-dispersive spectrometer. TEM investigations were carried out on a JEM–4000FX microscope at an accelerating voltage of 400 kV. TEM was used to investigate the crystal structure of the film especially at the interface and to look for possible Mn clusters. TEM was also used to measure the grain size in pure and doped ZnO films. XRD data were obtained on Siemens diffractometer (Fe Kα radiation with $\lambda = 0.193728$ nm) with a graphite monochromator and line-position-sensitive gas flow detector. Calculation of the grain size, d, was done using the angle dependence of the peak broadening.[10]

3. Results and discussion

In Fig. 1a the bright field high-resolution electron micrograph is shown for the nanograined ZnO thin film. The electron diffraction pattern is shown in Fig. 1b. The deposited ZnO film is dense, non-porous, nanograined, uniform, and non-textured. The grain size in this film is about 20 nm. In other Mn-doped samples the grain size was 20 ± 5 nm. In Fig. 2 two XRD spectra are shown, namely for pure ZnO (bottom) and ZnO doped by 40 at% MnO. Only wurtzite lines are visible in the pure ZnO film (ICPDS

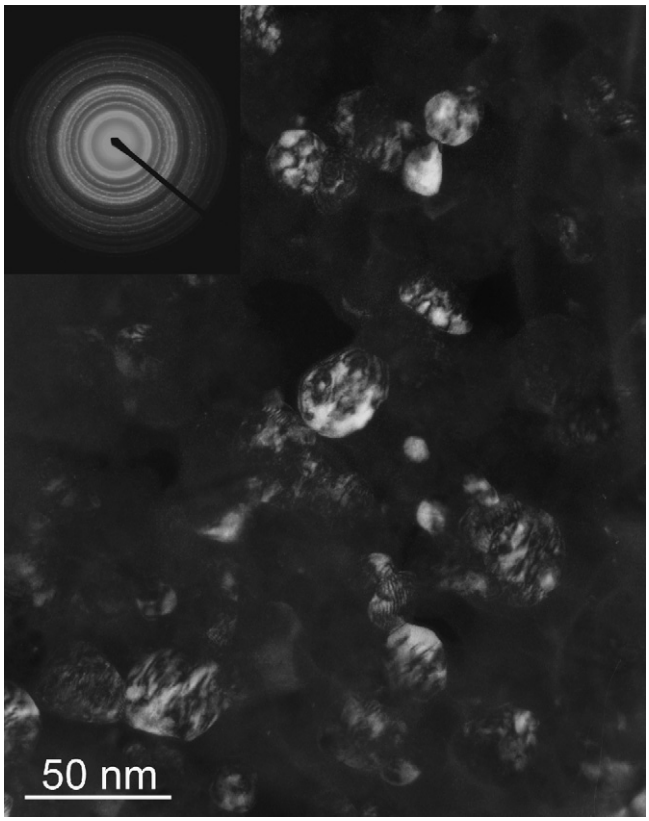

Fig. 1. Dark field TEM micrograph of the nanograined ZnO thin film deposited by the liquid ceramics technology and electron diffraction pattern as an inset. No texture is visible.

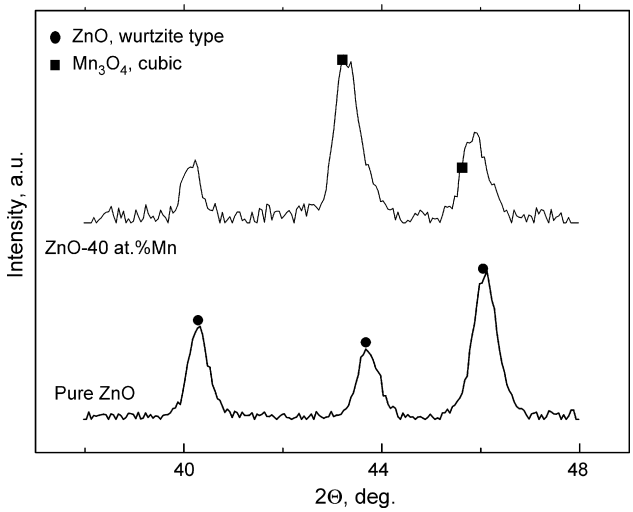

Fig. 2. XRD spectra for pure ZnO (bottom) and ZnO doped by 40 at% MnO. Only wurzite lines are visible in the pure ZnO film (ICPDS Card No. 36-1451). The cubic Mn_3O_4 phase (ICPDS Card No. 04-0732) appears additionally in the ZnO–40 at% MnO sample.

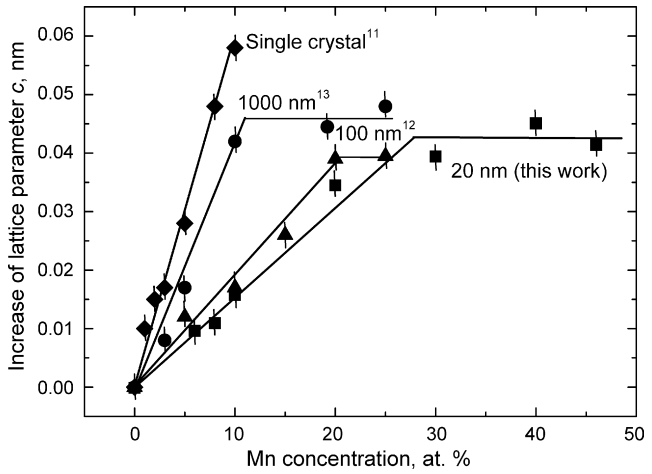

Fig. 3. Dependence of increase of lattice parameter c in Mn-doped ZnO films on the Mn-concentration. Full squares: our data ($d = 20$ nm). Diamonds: Mn-doped epitaxial films on the single crystalline ZnO substrate.[11] Circles: films with $d = 100$ nm obtained by the chemical spray pyrolysis.[12] Triangles: films with $d = 1000$ nm deposited by the MBE on the sapphire substrate.[13]

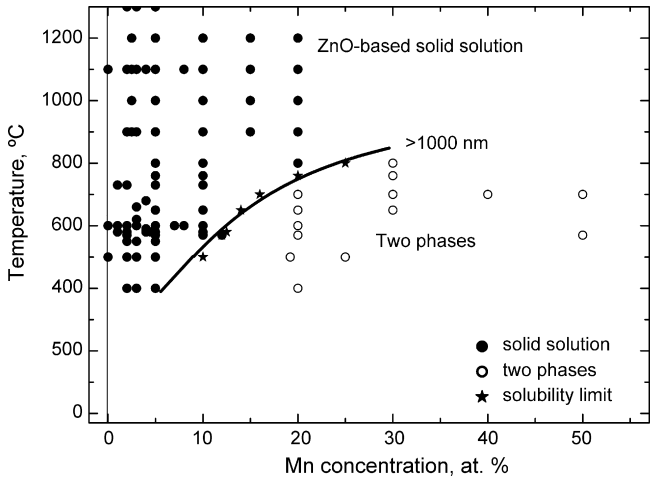

Fig. 4. Solubility limit of Mn in ZnO polycrystals with grain sizes above 1000 nm.[11–19]

Card No. 36-1451). The cubic Mn_3O_4 phase (ICPDS Card No. 04-0732) appears additionally in the ZnO–40 at% MnO sample. In Fig. 3 the increase of the lattice parameter c in the Mn-doped ZnO films with increasing Mn-concentration is shown. The error bars in Fig. 3 are defined by the angular error for the peak positions in XRD spectra. Both our data ($d = 20$ nm, diamonds) and the data taken from the literature are shown (Mn-doped epitaxial films on the single crystalline ZnO substrate,[11] squares; films with $d = 100$ nm obtained by the chemical spray pyrolysis,[12] circles; films with $d = 1000$ nm obtained by the molecular beam epitaxy (MBE) on the sapphire substrate,[13] triangles). The lattice spacing linearly increases up to the certain concentration c_{sa}. Above c_{sa}, the second phase Mn_3O_4 with cubic structure appears and the lattice spacing in the wurzite ZnO phase ceases to increase. The slope of the inclined portion of the curves decreases with decreasing grain size. It means that the solubility limit c_{sa} in the Mn-doped ZnO thin films with grain size 20 nm is about 33 at% Mn at 550 °C. The solubility limit in the bulk c_s is about 12 at% Mn at 550 °C.[14]

In order to find ferromagnetism in doped ZnO, it is important to ensure that it does not contain any particles of the second phase which could influence the sample's magnetic properties. In other words, it is essential that all published articles include data on the dopant concentration and presence or absence of the second phase. Usually, the presence or absence of a second phase is controlled by XRD. Measurable X-ray peaks appear in the diffraction spectra when the amount of a second phase is about 1–2%. TEM allows one to detect a second phase at lower content than XRD. However, such data are seldom present in the papers devoted to the magnetic behaviour of ZnO. Also, the usage of unified method (XRD) allows us to compare the data from different works and to bring them together in the same plot.

The majority of published works allows us to estimate the grain or particle size and to assign the data to a certain temperature, either that of a synthesis or that of the last thermal treatment. The published data encompass a grain (particle) size D of between 1 mm and 10 nm and temperatures from 300 to 1500 K. This gave us the unique chance to construct the $c_{sa}(T)$ dependencies for the broad interval of D and to compare the influence of internal boundaries and surfaces. The biggest data arrays exist for Co- and Mn-doped ZnO. In this work we will analyse the Mn-doped ZnO.

In Fig. 4 the solubility (solvus) limit of Mn in ZnO polycrystals is drawn using the data on polycrystals with a grain size above 1000 nm.[10–19] (The errors in Fig. 4, as well as in Figs. 5–7 are below the scale of the markers.) These samples were obtained by hydrothermal growth,[10] growth of Mn-doped epitaxial films on the single crystalline ZnO substrate,[11] pulsed laser and MBE deposition of the coarse-grained thin films on the sapphire substrate,[12,15] sintering of conventional powders,[16,17] co-precipitation,[18] growth of Mn-doped bulk crystals from oxalate precursors.[19] The solubility of Mn in ZnO reaches about 30 at% at 800 °C and falls to 5 at% at 400 °C. This line corresponds to the solubility in the volume of ZnO, the number of Mn atoms segregated in grain boundaries is negligible.

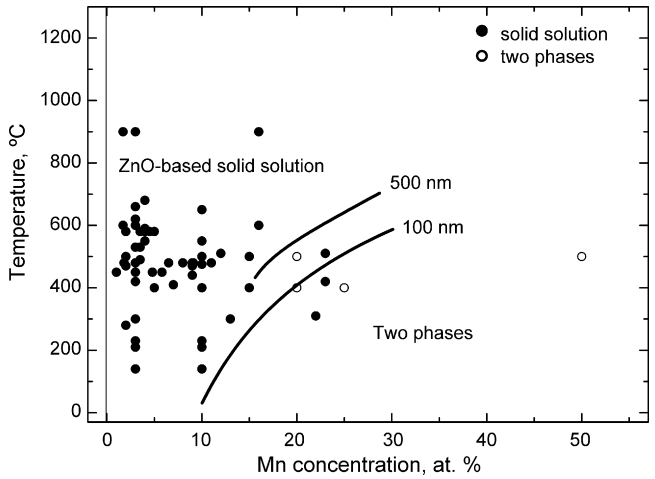

Fig. 5. Solubility limit of Mn in ZnO polycrystals with grain sizes between 100 and 1000 nm.[13,15,20–27]

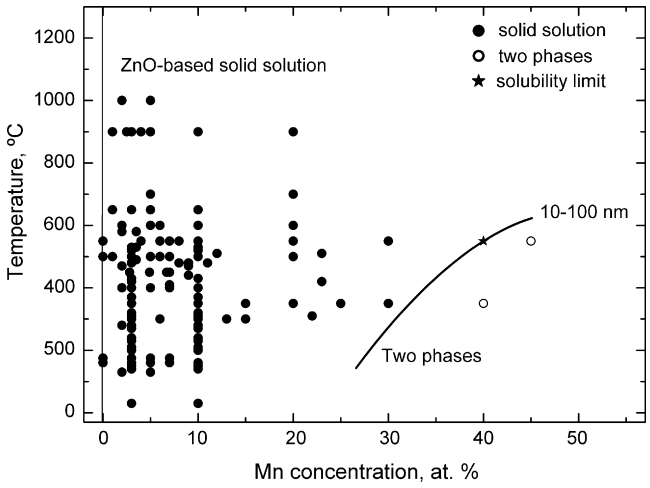

Fig. 6. Solubility limit of Mn in ZnO polycrystals with grain sizes between 10 and 100 nm.[15,16,20,21,28–38]

In Fig. 5 the solubility limit (solvus) of Mn in ZnO polycrystals is drawn using the data on polycrystals with grain size between 100 and 1000 nm.[13,15,20–27] These samples were obtained by the pulsed laser deposition (PLD) on the sapphire substrate,[15,20–22] Mn ion implantation into ZnO films deposited by PLD[23], sol–gel method[24], sintering fine powders,[25–27] and chemical spray pyrolysis.[13] The solubility of Mn in ZnO (for $D = 100$ nm) reaches about 25 at% at 500 °C and falls below 10 at% at room temperature. Mn solubility in polycrystals with grain size between 100 and 1000 nm is much higher than in the coarse-grained samples. For example at 600 °C it is two times higher.

In Fig. 6 the solubility limit (solvus) of Mn in ZnO polycrystals is drawn using the data on polycrystals with grain size between 10 and 100 nm.[15,16,20,28–38] These samples were obtained by the pulsed laser deposition,[15,16,20,21,28–31] full or partial sintering of very fine powders,[32–35] partial sintering of nanowires,[36,37] and magnetron sputtering.[38] The solubility of Mn in ZnO drastically increased in comparison with Fig. 4. It

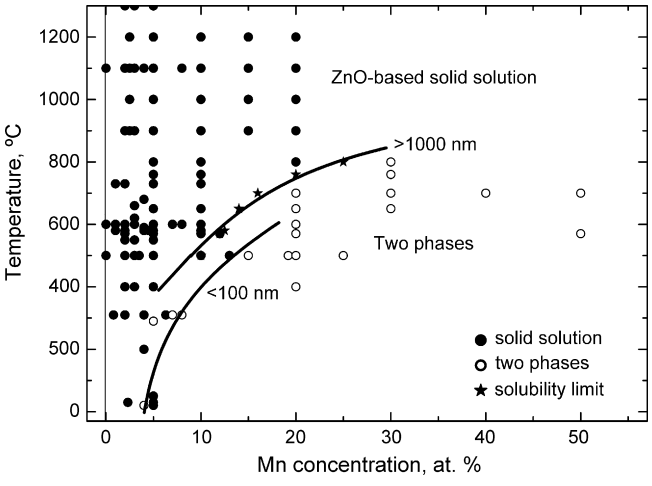

Fig. 7. Solubility limit of Mn in ZnO powders with various particle sizes.[11–19,39–46]

reached about 45 at% at 600 °C and remained above 20 at% at room temperature.

In Fig. 7 the solubility limit (solvus) of Mn in ZnO single crystals is drawn using the data on powder samples with different particle size.[11–19,39–46] The data are much scarcer in comparison with polycrystals (Figs. 4–6). The single crystals, particles, rods, wires etc. without GBs were obtained by hydrothermal growth,[14] growth of Mn-doped epitaxial films on the single crystalline ZnO substrate,[11] pulsed laser and MBE deposition of the coarse-grained thin films on the sapphire substrate,[12,15] sintering of conventional powders,[16,17] co-precipitation,[18] growth of Mn-doped bulk crystals from oxalate precursors,[19] condensation of nanopowders and nanowires from solution and vapour phase,[39–43] autocombustion,[44] ball milling of micro- and nanopowders,[45] sol–gel synthesis.[46] The solubility lines for the particle size above 1000 nm and below 100 nm are shown in Fig. 7. For large crystals (particles and/or grains larger than 1000 nm) the solubility limit line is the same as in Fig. 4 and corresponds to the bulk solidus. It is visible that the decrease of particle size also leads to the increase of the Mn solubility in ZnO. However, in this case c_{sa} shifts to the right much weaker than in Figs. 5 and 6 (poreless polycrystals). This difference demonstrates that GBs in ZnO can accumulate much more Mn atoms than free surfaces.

Based on the knowledge that Mn solubility depends on grain and particle size (Figs. 4–7), it is possible to estimate the maximum Mn segregation in ZnO GBs and free surfaces. Let us calculate first the area to volume ratio for the grains and particles. If we suppose that grains and particles are spheres with diameter D, the surface for each particle is πD^2 and the GB area for each grain is $\pi D^2/2$ (since each GB is shared between two neighbouring grains). The volume for spherical grains and particles is the same, namely $\pi D^3/6$. Thus the area to volume ratio, A, for the free surfaces of spherical particles is $A_{FS} = 3/D$ and for GBs of spherical grains $A_{GB} = 3/2D$. One of the earliest studies of grain shape was made by Lord Kelvin in 1887.[47] He showed that the optimal space-filling grain shape, with a minimal surface area and surface tension, is a polyhedron known as a tetrakaidecahedron, which has 14 faces, 24 corners and 36 edges. Tetrakaidecahedron is an octahedron truncated by cube. For the Kelvin tetrakaidecahedron the ratio of surface area to that of a sphere of the same volume is 1.099.[47] Thus the area to volume ratio for grains is $A_{GB} = 1.65/D$. If one monolayer (ML) of Mn covers ZnO free surfaces or GBs, their input, c_{FS} or c_{GB}, in the full concentration can be calculated as a product of A_{FS} or A_{GB} and the thickness, t, of a surface or GB layer. Lattice constant of ZnO wurtzite lattice d can be estimated as the cubic root from the unit cell volume. The unit cell volume for ZnO is about $47 \cdot 10^{-3}$ nm^3 according to our measurements. Thus $d = 0.36$ nm. Therefore, for the one monolayer $t = d$, $c_{FS} = d\,A_{FS} = 1.08/D$ and $c_{GB} = d\,A_{GB} = 0.59/D$.

In Fig. 8 the input of Mn accumulated in GBs and surfaces in total concentration is shown for different grain size. c_{FS} and c_{GB} values for 1 ML are shown by thin and thick straight lines, respectively, with a slope of −1 in the bottom part of the Fig. 8. The solubility limit of Mn in the single-crystalline or

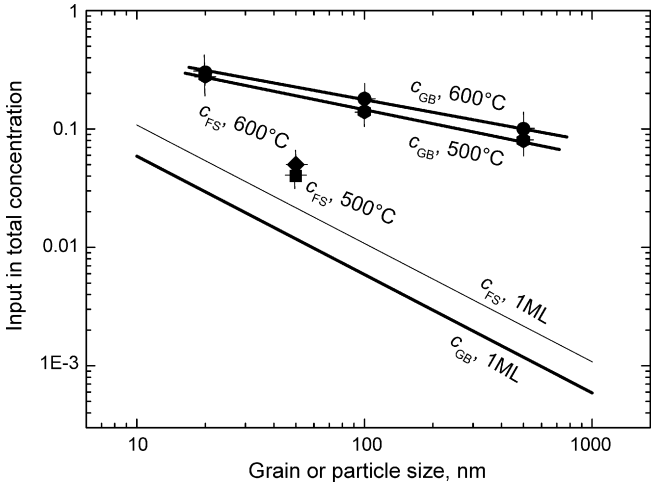

Fig. 8. Size dependence of the input of GB or surface Mn segregation into full Mn content.

coarse-grained ZnO at 500 °C and 600 °C is 9 and 12 at% Mn, respectively (Fig. 4). If we subtract these values from the solubility limit of Mn in the fine-grained ZnO (Figs. 5–7), we obtain the input of GB, c_{GB}, or free surface segregation, c_{FS}, into total Mn solubility in the ZnO polycrystals. The c_{GB} values are shown in Fig. 8 by full circles (500 °C) and full hexagons (600 °C). It is easy to see that the experimental c_{GB} values are more than one order of magnitude higher than the calculated values for 1 ML. Moreover, the slope of the lines for GB input is slightly lower than −1. It means that the GB input in the total Mn concentration increases with decreasing grain size. This fact undoubtedly indicates the multilayer GB Mn segregation in ZnO. The c_{FS} points for free surfaces (full square and full diamond) lie lower than the c_{GB} values for GBs. It means that free surfaces can accumulate much less Mn in comparison with GBs.

Fig. 8 undoubtedly indicates that the Mn enrichement of GBs in fine-grained ZnO cannot be reduced to the simple single-layer GB segregation analysed by McLean.[1] Such layers of a GB phase of a finite thickness of few nm were first observed and theoretically treated with the aid of force-balance models in the pioneering works of David A. Clarke on silicon nitride.[48–51] Later, nanometer-thick, disordered films of a nearly constant or "equilibrium" thickness have been frequently observed in GBs in ceramics[49–61] and oxide/metal interfaces.[62–64] Thin equlibrium GB or surface films in the one-phase area of a bulk phase diagram were first considered by J.W. Cahn.[65] He proposed the idea that the transition from incomplete to complete surface wetting is a phase transformation. Later this idea was successfully applied for GBs, and also old data on GB wetting were reconsidered from this point of view.[66–68] GB wetting phase transformation proceeds at the temperature T_{wGB} where GB energy σ_{GB} becomes equal to the energy $2\sigma_{SL}$ of two solid/liquid interfaces. Above T_{wGB} GB is substituted by a layer of the melt. The tie-line of the GB wetting phase transition in the two-phase area of a bulk phase diagram continues into the one-phase area as a prewetting (or GB solidus) line. In the area between GB solidus and bulk solidus, GB contains the thin layer of a GB phase. The energy gain (σ_{GB}–$2\sigma_{SL}$) above T_{wGB} permits to stabilize such thin layer of a GB phase between the abutting crystals. Such phase is metastable in the bulk but become stable in the GB. The formation of GB phase layer of thickness l leads to the energy loss $l\Delta g$. Finite thickness l of the GB phase is defined by the equality of the energy gain (σ_{GB}–$2\sigma_{SL}$) and energy loss $l\Delta g$. In this simplest model, the prewetting GB layer of finite thickness l suddenly appears by crossing the prewetting (GB soludus) line $c_{bt}(T)$. The direct evidence for the existence of such a first-order prewetting transition (i.e., a finite jump in film thickness) has been recently reported for oxide surfaces.[69] Thickness l logarithmically diverges close to the bulk solidus. It is due to the fact that the thickness of a wetting phase is thermodynamically infinite in the two-phase area. Physically, in the two-phase area, its thickness is defined only by the amount of the wetting phase. Several ML thick liquid-like GB layers possessing high diffusivity were observed in the Cu–Bi,[70–73] Al–Zn,[74–76] Fe–Si–Zn[77–80] and W–Ni alloys.[81,82] The direct HREM evidence for thin GB films and triple junction "pockets" of has been recently obtained in metallic W–Ni[80,81] and Al–Zn[72] alloys. The recent work performed with computation thermodynamics methods demonstrated that a nanoscale quasi-liquid GB film can be thermodynamically stable at as low as 60-85% of bulk solidus temperatures.[83]

Later, the Cahn's critical point wetting model has been developed further and generalized.[84–86] It is not excluded that in the nanograined ZnO–MnO polycrystals the situation is more complicated than the simple sequence "monolayer adsorption → interfacial film → macroscopically thick complete wetting film". Additional copmplexity comes from the possible occurrence of GB roughening,[72] GB layering,[87] pseudo-partial (or frustrated-complete) melting/wetting,[88] first order or continous adsorption/wetting transitions,[89] and interfacial critical points.[76,77] Good examples can be found on the recent works on GB phase transitions in alumina.[90–92] The nanometer-thick GB films of a nearly constant or "equilibrium" thickness have been widely observed in ZnO doped by Bi_2O_3.[52,53,88–100] ZnO doped by Bi is used for varistors manufacturing. Varistors exhibit highly non-linear current–voltage characteristics with a high resistivity below a threshold electric field, becoming conductive when this field is exceeded. This phenomenon enables them to be used in current over-surge protection circuits.[100,101] After liquid-phase sintering, such material consists of ZnO grains separated by thin Bi_2O_3-rich GB layers. Interfaces between ZnO grains control the non-linear current-voltage characteristics. The presence of a few nm-thick Bi-rich GB phase in ZnO is governed by the GB wetting phase transformation. The liquid-like GB films have also been found in cases of subsolidus activated sintering.[61] In fact, enhanced diffusion in these liquid-like GB films was used to explain the mysterious subsolidus activated sintering mechanism.[61,81] It is interesting, that along with the simplest Cahn model of the transition from partially wetted GBs to completely wetted ones, more complicated situation was also observed in the ZnO–Bi_2O_3 system, namely the transition from pseudo-partially wetted GBs to the completely wetted ones.[88] In this case thin GB layer may exist in the equilibrium with thick Bi_2O_3 droplets having non-zero contact angle in the GB plane.

The logarithmic divergence of the GB layer thickness predicted by Cahn model may be the reason for the high value of GB thickness obtained from Fig. 8. The lines in Fig. 8 were calculated based on the apparent shift of the solubility. Therefore, the resulting GB thickness corresponds to that at the solubiluty (solvus) line. Few nm thick Bi-rich layers were observed also in the ZnO surfaces.[102–104] Their thickness was close to that of GB layers.[88–94] The thickness of surficial films was explained by the pseudo-partial (frustrated-complete) surface wetting.[104] In case of the frustrated-complete wetting, the thickness of a surficial (or GB) film also increases with increasing dopant concentration (activity) and can reach few monolayers. However, it does not diverge by approaching the solubility limit line like GB (or surficial) films in case of complete wetting and remains finite.[87,102,105] In the case of Mn-doped ZnO, the estimation presented in Fig. 8 predicts lower Mn-capacity of free surfaces in comparison with GBs. This fact has to be carefully investigated in the future experiments. It may be the indication of complete wetting in GBs and frustrated-complete wetting in surfaces. Recent observation of thin GB layers of the Fe-rich phase in the Fe-doped nanograined ZnO also increases the success chances in searching the Mn-enriched GB layers in ZnO.[106] Therefore, based on the results obtained in this work one can expect to observe in the future various interesting GB phases and phase trasnformations in the Mn-doped ZnO. Furthermore, the observed shift of the solvus line in the Mn-doped ZnO will also permit to explain the mysterious phenomenon of the room-temperature ferromagnetism in the broad-band transparent semiconductor ZnO.

4. Conclusions

1. The accumulation of Mn in grain boundaries and free surfaces drastically shifts the line of Mn solubility limit in ZnO to the higher Mn concentrations. For example, at 550 °C the total solubility in the bulk is about 10 at% Mn and in the nanograined sample with grain size below 20 nm it is about 40 at% Mn.

2. Small grain size leads to the larger shift when compared with similarly small particle sizes. This means that the Mn accumulation ability of grain boundaries is about 2–4 times higher than that of free surfaces.

3. Thus, the phase diagrams for the materials having a grain size below 1000 nm have to be re-investigated. An especially drastic change to the phase diagrams results when the grain size is below 100 nm.

Acknowledgements

Authors thank the Russian Foundation for Basic Research (grants 08-08-90105, 08-08-91302 and 09-08-90406), Deutsche akademische Austauschdienst (DAAD), Deutsche Forschungsgemeinschaft (DFG) and German federal ministry for education and science (BMBF) for the financial support of investigations and exchange travel. Authors cordially thank Prof. G. Schütz, Dr. D. Goll and Dr. E. Goering for stimulating discussions, Dr. A. Nekrasov for the help with EPMA measurements, and Ms. J. Breithaupt for improving the English.

References

1. McLean, D., *Grain Boundaries in Metals*. Clarendon Press, Oxford, 1957, pp. 109–123.
2. Beke, D. L., Cserháti, C., Erdélyi, Z. and Szabó, I. A., Segregation in nanostructures. In *Nanoclusters and Nanocrystals*, ed. H. S. Nalwa. American Scientific Publishers, Valencia, CA, 2002, pp. 1–47.
3. Beke, D. L., Erdélyi, Z., Bakos, P., Cserháti, C. and Szabó, I. A., Segregation induced phase transformations in nanostructures. In *Proceedings of the International Conference Solid–Solid Phase Transformations '99 (JIMIC-3)*, ed. M. Koiwa, K. Otsuka and T. Miyazaki, 1999, pp. 1297–1300.
4. Weissmuller, J. and Lemier, Chr., On the size dependence of the critical point of nanoscale interstitial solid solutions. *Phil. Mag. Lett.*, 2000, **80**, 411–418.
5. Lartigue-Korinek, S., Legros, C., Carry, C. and Herbst, F., Titanium effect on phase transformation and sintering behavior of transition alumina. *J. Eur. Ceram. Soc.*, 2006, **26**, 2219–2230.
6. Gülgün, M. A., Voytovych, R., Maclaren, I., Rühle, M. and Cannon, R. M., Cation segregation in an oxide ceramic with low solubility: Yttrium doped α-alumina. *Interf. Sci.*, 2002, **10**, 99–110.
7. Wang, Q., Lian, G. and Dickey, E. C., Grain boundary segregation in yttrium-doped polycrystalline TiO_2. *Acta Mater.*, 2004, **52**, 809–820.
8. Terwilliger, C. D. and Chiang, Y. M., Size-dependent solute segregation and total solubility in ultrafine polycrystals: Ca in TiO_2. *Acta Metall. Mater.*, 1995, **43**, 319–328.
9. Dietl, T., Ohno, H., Matsukura, F., Cibert, J. and Ferrand, D., Zener model description of ferromagnetism in zinc-blende magnetic semiconductors. *Science*, 2000, **287**, 1019–1022.
10. Soyer, A., FHKL—a program to compute rocking curves and crystallographic data of interest for the dynamical theory of X-rays. *J. Appl. Crystallogr.*, 1995, **28**, 244–247.
11. Masuko, K., Ashida, A., Yoshimura, T. and Fujimura, N., Preparation and the magnetic property of ZnMnO thin films on (0 0 0 1) ZnO single crystal substrate. *J. Magn. Magn. Mater.*, 2007, **310**, E711–E713.
12. Mofor, A. C., El-Shaer, A., Bakin, A., Wehmann, H.-H., Ahlers, H., Siegner, U. *et al.*, Magnetic property investigations on ZnMnO. *Superlatt. Microstruc.*, 2006, **39**, 381–386.
13. Reddy, L. R., Prathap, P., Subbaiah, Y. P. V., Reddy, K. T. R. and Yi, J., Structural and optical properties of sprayed $Zn_{1-x}Mn_xO$ films. *Solid State Sci.*, 2007, **9**, 718–721.
14. Bates, C. H., White, W. B. and Roy, R., The solubility of transition metal oxides in zink oxide and the reflectance spectra of Mn^{2+} and Fe^{2+} in tetrahedral fields. *J. Inorg. Nucl. Chem.*, 1966, **28**, 397–405.
15. Diaconu, M., Schmidt, H., Hochmuth, H., Lorenz, M., Benndorf, G., Spemann, D. *et al.*, Room-temperature ferromagnetic Mn-alloyed ZnO films obtained by pulsed laser deposition. *J. Magn. Magn. Mater.*, 2006, **307**, 212–221.
16. Kolesnik, S., Dabrowski, B. and Mais, J., Structural and magnetic properties of transition metal substituted ZnO. *J. Appl. Phys.*, 2004, **95**, 2582–2586.
17. Kolesnik, S. and Dabrowski, B., Absence of room temperature ferromagnetism in bulk Mn-doped ZnO. *J. Appl. Phys.*, 2004, **96**, 5379–5381.
18. Peiteado, M., Caballero, A. C. and Makovec, D., Phase evolution of $Zn_{1-x}Mn_xO$ system synthesized via oxalate precursors. *J. Europ. Ceram. Soc.*, 2007, **27**, 3915–3918.
19. Lawes, G., Risbud, A. S., Ramirez, A. P. and Seshadi, R., Absence of ferromagnetism in Co and Mn substituted polycrystalline ZnO. *Phys. Rev. B*, 2005, **71**, 045201, 5 pp.
20. Pradhan, A. K., Hunter, D., Zhang, K., Dadson, J. B., Mohanty, S., Williams, T. M. *et al.*, Magnetic and spectroscopic characteristics of ZnMnO system. *Appl. Surf. Sci.*, 2005, **252**, 1628–1633.
21. Schmidt, H., Diaconu, M., Hochmuth, H., Lorenz, M., Setzer, A., Esquinazi, P. *et al.*, Weak ferromagnetism in textured $Zn_{1-x}(TM)_xO$ thin films. *Superlatt. Microstruc.*, 2006, **39**, 334–339.
22. Diaconu, M., Schmidt, H., Hochmuth, H., Lorenz, M., Benndorf, G., Lenzner, J. *et al.*, UV optical properties of ferromagnetic Mn-doped ZnO thin films grown by PLD. *Thin Solid Films*, 2005, **486**, 117–121.

23. Venkataraj, S., Ohashi, N., Sakaguchi, I., Adachi, Y., Ohgaki, T., Ryoken, H. *et al.*, Structural and magnetic properties of Mn-ion implanted ZnO films. *J. Appl. Phys.*, 2007, **102**, 014905, 7 pp.
24. Maiti, U. N., Ghosh, P. K., Nandy, S. and Chattopadhyay, K. K., Effect of Mn doping on the optical and structural properties of ZnO nano/microfibrous thin film synthesized by sol–gel technique. *Phys. B*, 2007, **387**, 103–108.
25. Bhatti, K. P., Chaudhary, S., Pandya, D. K. and Kashyap, S. C., Extrinsic nature of the room temperature ferromagnetism in $(ZnO)_{1-x}(MnO_2)_x$ for $0.01 \leq x \leq 0.97$. *Solid State Comm.*, 2006, **140**, 23–27.
26. Costa-Kramer, J. L., Briones, F., Fernandez, J. F., Caballero, A. C., Villegas, M., Díaz, M. *et al.*, Nanostructure and magnetic properties of the MnZnO system, a room temperature magnetic semiconductor? *Nanotechnology*, 2005, **16**, 214–218.
27. Pal, M. and Pal, M., Nanocrystalline Mn-doped ZnO prepared by chemical route. *Jap. J. Appl. Phys.*, 2005, **44**, 7901–7903.
28. Li, X. Z., Zhang, J. and Sellmyer, D. J., Structural study of Mn-doped ZnO films by TEM. *Sol. State. Comm.*, 2007, **141**, 398–401.
29. Dhananjay, A., Nagaraju, J. and Krupanidhi, S. B., Dc and ac transport properties of Mn-doped ZnO thin films grown by pulsed laser ablation. *J. Mater. Sci. Eng. B*, 2006, **133**, 70–76.
30. Samanta, K., Dussan, S., Katiyar, R. S. and Bhattacharya, P., Structural and optical properties of nanocrystalline $Zn_{1-x}Mn_xO$. *Appl. Phys. Lett.*, 2007, **90**, 261903, 3 pp.
31. Savchuk, A. I., Gorley, P. N., Khomyak, V. V., Ulyanytsky, K. S., Bilichuk, S. V., Perrone, A. *et al.*, ZnO-based semimagnetic semiconductors: growth and magnetism aspects. *Mater. Sci. Eng. B*, 2004, **109**, 196–199.
32. Barick, K. C. and Bahadur, D., Synthesis, self-assembly, and properties of Mn doped ZnO nanoparticles. *J. Nanosci. Nanotechnol.*, 2007, **7**, 1935–1940.
33. Jayakumar, O. D., Salunke, H. G., Kadam, R. M., Mohapatra, M., Yaswant, G. and Kulshreshtha, S. K., Magnetism in Mn-doped ZnO nanoparticles prepared by a co-precipitation method. *Nanotechnology*, 2006, **17**, 1278–1285.
34. Alaria, J., Turek, P., Bernard, M., Bouloudenine, M., Berbadj, A., Brihi, N. *et al.*, No ferromagnetism in Mn doped ZnO semiconductors. *Chem. Phys. Lett.*, 2005, **415**, 337–341.
35. Mandal, S. K., Das, A. K., Nath, T. K., Karmakar, D. and Satpati, B., Microstructural and magnetic properties of ZnO:TM (TM = Co,Mn) diluted magnetic semiconducting nanoparticles. *J. Appl. Phys.*, 2006, **100**, 104315, 8 pp.
36. Kang, Y. J., Kim, D. S., Lee, S. H., Park, J., Je, J. C., Moon, Y. *et al.*, Ferromagnetic $Zn_{1-x}Mn_xO$ ($x = 0.05$, 0.1, and 0.2) nanowires. *J. Phys. Chem. C*, 2007, **111**, 14956–14961.
37. Cong, C. J. and Zhang, K. L., Influence of Mn valence bond on ferromagnetic properties of corn-like $Zn_{1-x}Mn_xO$ nanorods. *Phys. Stat. Sol. B*, 2006, **243**, 2764–2771.
38. Kim, D. S., Lee, S., Min, C., Kim, H. M., Yuldashev, S. U., Kang, T. W. *et al.*, Formation and characterization of $(Zn_{1-x}Mn_x)O$ diluted magnetic semiconductors grown on (0 0 0 1) Al_2O_3 substrates. *Jap. J. Appl. Phys.*, 2003, **42**, 7217–7221.
39. Sarma, D. D., Viswanatha, R., Sapra, S., Prakash, A. and García-Hernádez, M. J., Magnetic properties of doped II-VI semiconductor nanocrystals. *Nanosci. Nanotechnol.*, 2005, **5**, 1503–1508.
40. Clavel, G., Pinna, N. and Zitoun, D., Magnetic properties of cobalt and manganese doped ZnO nanowires. *Phys. Stat. Sol. A*, 2007, **204**, 118–124.
41. Glaspell, G., Dutta, P. and Manivannan, A., A room-temperature and microwave synthesis of M-doped ZnO (M = Co, Cr, Fe, Mn & Ni). *J. Cluster Sci.*, 2005, **16**, 523–536.
42. Chang, Y. Q., Wang, D. B., Luo, X. H., Xu, X. Y., Chen, X. H., Li, L. *et al.*, Synthesis, optical, and magnetic properties of diluted magnetic semiconductor $Zn_{1-x}Mn_xO$ nanowires via vapor phase growth. *Appl. Phys. Lett.*, 2003, **83**, 4020–4022.
43. Meron, T. and Markovich, G., Ferromagnetism in colloidal Mn^{2+}-doped ZnO nanocrystals. *J. Phys. Chem. B*, 2005, **109**, 20232–20236.
44. Deka, S. and Joy, P. A., Ferromagnetism induced by hydrogen in polycrystalline nonmagnetic $Zn_{0.95}Co_{0.05}O$. *Sol. State. Comm.*, 2007, **142**, 190–194.
45. Bartolome, F., Blasco, J., García, L. M., García, J., Jiménez, S. and Lozano, A., Is ball milling a worthy route to produce magnetic semiconductors? *J. Magn. Magn. Mater.*, 2007, **316**, E195–E198.
46. Thota, S., Dutta, T. and Kumar, J., On the sol–gel synthesis and thermal, structural, and magnetic studies of transition metal (Ni, Co, Mn) containing ZnO powders. *J. Phys. Cond. Mater.*, 2006, **18**, 2473–2486.
47. Hosford, W. F., *Materials Science: An Intermediate Text*. Cambridge University Press, Cambridge etc., 2007, pp. 7–9.
48. Clarke, D. R., On the equilibrium thickness of intergranular glass phases in ceramic materials. *J. Amer. Ceram. Soc.*, 1987, **70**, 15–22.
49. Clarke, D. R., Shaw, T. M., Philipse, A. P. and Horn, R. G., Possible electrical double-layer contribution to the equilibrium thickness of intergranular glass films in polycrystalline ceramics. *J. Amer. Ceram. Soc.*, 1993, **76**, 1201–1204.
50. Tanaka, I., Kleebe, H.-J., Cinibulk, M. K., Bruley, J., Clarke, D. R. and Rühle, M. J., Calcium concentration dependence of the intergranular film thickness in silicon nitride. *Amer. Ceram. Soc.*, 1994, **77**, 911–914.
51. Bobeth, M., Clarke, D. R. and Pompe, W., A diffuse interface description of intergranular films in polycrystalline ceramics. *J. Amer. Ceram. Soc.*, 1999, **82**, 1537–1546.
52. Lee, J.-R., Chiang, Y.-M. and Ceder, G., Pressure-thermodynamic study of grain boundaries: Bi segregation in ZnO. *Acta Mater.*, 1997, **45**, 1247–1257.
53. Wang, H. and Chiang, Y.-M., Thermodynamic stability of intergranular amorphous films in bismuth-doped zinc oxide. *J. Amer. Ceram. Soc.*, 1998, **81**, 89–96.
54. Kleebe, H.-J., Hoffman, M. J. and Rühle, M., Influence of secondary phase chemistry on grain boundary film thickness in silicon nitride. *Z. Metallkd.*, 1992, **83**, 610–617.
55. Kleebe, H.-J., Cinibulk, M. K., Cannon, R. M. and Rühle, M., Statistical analysis of the iIntergranular film thickness in silicon nitride ceramics. *J. Amer. Ceram. Soc.*, 1993, **76**, 1969–1977.
56. Chiang, Y.-M., Silverman, L. A., French, R. H. and Cannon, R. M., Thin glass film between ultrafine conductor particles in thick-film resistors. *J. Amer. Ceram. Soc.*, 1994, **77**, 1143–1152.
57. Ackler, H. D. and Chiang, Y.-M., Model experiment on thermodynamic stability of retained intergranular amorphous films. *J. Amer. Ceram. Soc.*, 1997, **80**, 1893–1896.
58. Chiang, Y.-M., Wang, H. and Lee, J.-R., HREM and STEM of intergranular films at zinc oxide varistor grain boundaries. *J. Microsci.*, 1998, **191**, 275–285.
59. Ackler, H. D. and Chiang, Y.-M., Model experiment on thermodynamic stability of retained intergranular amorphous films. *J. Am. Ceram. Soc.*, 1999, **82**, 183–196.
60. Cannon, R. M. and Esposito, L., High temperature colloidal behaviour: particles in liquid silicates. *Z. Metallkd.*, 1999, **90**, 1002–1015.
61. Luo, J., Wang, H. and Chiang, Y.-M., Origin of solid-state activated sintering in Bi_2O_3-doped ZnO. *J. Am. Ceram. Soc.*, 1999, **82**, 916–920.
62. Avishai, A., Scheu, C. and Kaplan, W. D., Interganular films at metal-ceramic interfaces. Part 1—interface structure and chemistry. *Acta Mater.*, 2005, **53**, 1559–1569.
63. Levi, G. and Kaplan, W. D., The influence of interfacial wetting and adhesion on the formation of voids at metal-ceramic interfaces. *J. Mater. Sci.*, 2006, **41**, 817–821.
64. Baram, M. and Kaplan, W. D., Intergranular films at Au-sapphire interfaces. *J. Mater. Sci.*, 2006, **41**, 7775–7784.
65. Cahn, J. W., Wetting transition on surface. *J. Chem. Phys.*, 1977, **66**, 3667–3679.
66. Eustathopoulos, N., Energetics of solid/liquid interfaces of metals and alloys. *Int. Met. Rev.*, 1983, **28**, 189–210.
67. Straumal, B., Muschik, T., Gust, W. and Predel, B., The wetting transition in high and low energy grain boundaries in the Cu(In) system. *Acta Metall. Mater.*, 1992, **40**, 939–945.
68. Straumal, B., Molodov, D. and Gust, W., Tie lines of the grain boundary wetting phase transition in the Al–Sn system. *J. Phase Equilibria*, 1994, **15**, 386–391.

69. Qian, H. and Luo, Nanoscale surficial films and a surface transition in V_2O_5–TiO_2-based ternary oxide systems. *J. Acta Mater.*, 2008, **56**, 4702–4714.
70. Divinski, S. V., Lohmann, M., Herzig, Chr., Straumal, B., Baretzky, B. and Gust, W., Grain boundary melting phase transition in the Cu–Bi system. *Phys. Rev. B*, 2005, **71**, 104104, 8 pp.
71. Chang, L.-S., Rabkin, E., Straumal, B. B., Baretzky, B. and Gust, W., Thermodynamic aspects of the grain boundary segregation in Cu(Bi) alloys. *Acta mater*, 1999, **47**, 4041–4046.
72. Straumal, B. B., Polyakov, S. A., Chang, L.-S. and Mittemeijer, E. J., The effect of bismuth segregation on the faceting of Σ3 and Σ9 coincidence boundaries in copper bicrystals. *Int. J. Mater. Res.*, 2007, **98**, 451–456.
73. Straumal, B., Prokofjev, S. I., Chang, L.-S., Sluchanko, N. E., Baretzky, B., Gust, W. *et al.*, Grain boundary phase transitions in the Cu–Bi system. *Def. Diff. Forum.*, 2001, **194-199**, 1343–1348.
74. Straumal, B. B., Baretzky, B., Mazilkin, A. A., Phillipp, F., Kogtenkova, O. A., Volkov, M. N. *et al.*, Formation of nanograined structure and decomposition of supersaturated solid solution during high pressure torsion of Al–Zn and Al–Mg. *Acta Mater.*, 2004, **52**, 4469–4478.
75. Straumal, B. B., Mazilkin, A. A., Kogtenkova, O. A., Protasova, S. G. and Baretzky, B., Grain boundary phase observed in Al–5 at.% Zn alloy by using HREM. *Phil. Mag. Lett.*, 2007, **87**, 423–430.
76. Straumal, B. B., Kogtenkova, O. and Zięba, P., Wetting transition of grain boundary triple junctions. *Acta Mater.*, 2008, **56**, 925–933.
77. Rabkin, E. I., Semenov, V. N., Shvindlerman, L. S. and Straumal, B. B., Penetration of tin and zinc along tilt grain boundaries 43°[100] in Fe–5 at.%Si alloy: Premelting phase transition? *Acta metall. Mater.*, 1991, **39**, 627–639.
78. Noskovich, O. I., Rabkin, E. I., Semenov, V. N., Straumal, B. B. and Shvindlerman, L. S., Wetting and premelting phase transitions in 38°[100] tilt grain boundaries in (Fe–12 at.% Si)–Zn alloy in the vicinity of the A2-B2 bulk ordering in Fe–12 at.% Si alloy. *Acta metall. Mater.*, 1991, **39**, 3091–3098.
79. Straumal, B. B., Noskovich, O. I., Semenov, V. N., Shvindlerman, L. S., Gust, W. and Predel, B., Premelting transition on 38°<100> tilt grain boundaries in (Fe–10 at.% Si)–Zn alloys. *Acta metall. mater.*, 1992, **40**, 795–801.
80. Straumal, B., Rabkin, E., Lojkowski, W., Gust, W. and Shvindlerman, L. S., Pressure influence on the grain boundary wetting phase transition in Fe–Si alloys. *Acta mater.*, 1997, **45**, 1931–1940.
81. Gupta, V. K., Yoon, D. H., Meyer III, H. M. and Luo, J., Thin intergranular films and solid-state activated sintering in nickel-doped tungsten. *Acta Mater.*, 2007, **55**, 3131–3142.
82. Luo, J., Gupta, V. K., Yoon, D. H. and Meyer, H. M., Segregation-induced grain boundary premelting in nickel-doped tungsten. *Appl. Phys. Lett.*, 2005, **87**, 231902, 3 pp.
83. Luo, J. and Shi, X., Grain boundary disordering in binary alloys. *Appl. Phys. Lett.*, 2008, **92**, 101901, 3 pp.
84. Tang, M., Carter, W. C. and Cannon, R. M., Grain boundary transitions in binary alloys. *Phys. Rev. Lett.*, 2006, **97**, 075502, 4 pp.
85. Tang, M., Carter, W. C. and Cannon, R. M., Diffuse interface model for structural transitions of grain boundaries. *Phys. Rev. B*, 2006, **73**, 024102, 14 pp.
86. Luo, J., Tang, M., Cannon, R. M., Carter, W. C. and Chiang, Y.-M., Pressure-balance and diffuse-interface models for surficial amorphous films. *Mater. Sci. Eng., A*, 2006, **422**, 19–28.
87. Luo, J., Stabilization of nanoscale quasi-liquid interfacial films in inorganic materials: a review and critical assessment. *Crit. Rev. Solid State Mater. Sci.*, 2007, **32**, 67–101.
88. Luo, J., Chiang, Y.-M. and Cannon, R. M., Nanometer-thick surficial films in oxides as a case of prewetting. *Langmuir*, 2005, **21**, 7358–7365.
89. Straumal, B. B., Gornakova, A. S., Kogtenkova, O. A., Protasova, S. G., Sursaeva, V. G. and Baretzky, B., Continuous and discontinuous grain boundary wetting in the Zn–Al system. *Phys. Rev. B*, 2008, **78**, 054202, 6 pp.
90. Dillon, S. J. and Harmer, M. P., Multiple grain boundary transitions in ceramics: a case study of alumina. *Acta Mater.*, 2007, **55**, 5247–5254.
91. Dillon, S. J., Tang, M., Carter, W. C. and Harmer, M. P., Complexion: a new concept for kinetic engineering in materials science. *Acta Mater.*, 2007, **55**, 6208–6218.
92. Dillon, S. J. and Harmer, M. P., Demystifying the role of sintering additives with "complexion". *J. Europ. Ceram. Soc.*, 2008, **28**, 1485–1493.
93. Wong, J., Nature of intergranular phase in nonohmic ZnO ceramics containing 0.5 mol% Bi_2O_3. *J. Am. Ceram. Soc.*, 1974, **57**, 357–359.
94. Wong, J. and Morris, W. G., Microstructure and phases in nonohmic ZnO–Bi_2O_3 ceramics. *Am. Ceram. Soc. Bull.*, 1974, **53**, 816–820.
95. Greuter, F., Electrically active interfaces in ZnO varistor. *Solid State Ionics*, 1995, **75**, 67–78.
96. Gambino, J. P., Kingery, W. D., Pike, G. E. and Philipp, H. R., Effect of heat treatments on the wetting behavior of bismuth rich intergranular phases in ZnO:Bi:Co varistors. *J. Am. Ceram. Soc.*, 1989, **72**, 642–645.
97. Kingery, W. D., van der Sande, J. B. and Mitamura, T., A scanning transmission electron microscopy investigation of grain boundary segregation in a ZnO–Bi_2O_3 varistor. *J. Am. Ceram. Soc.*, 1979, **62**, 221–222.
98. Olsson, E., Falk, L. K. L. and Dunlop, G. L., The microstructure of a ZnO varistor material. *J. Mater. Sci.*, 1985, **20**, 4091–4098.
99. Olsson, E. and Dunlop, G. L., Characterization of individual interfacial barriers in a ZnO varistor material. *J. Appl. Phys.*, 1989, **66**, 3666–3675.
100. Matsuoka, M., Nonohmic properties of zinc oxide resistors. *Jpn. J. Appl. Phys.*, 1971, **10**, 736–738.
101. Straumal, B. B., Mazilkin, A. A., Straumal, P. B. and Myatiev, A. A., Distribution of impurities and minor components in nanostructured conducting oxides. *Int. J. Nanomanufact.*, 2008, **2**, 253–270.
102. Luo, J. and Chiang, Y.-M., Wetting and prewetting on ceramic surfaces. *Annu. Rev. Mater. Res.*, 2008, **38**, 227–249.
103. Luo, J. and Chiang, Y.-M., Existence and stability of nanometer-thick disordered films on oxide surfaces. *Acta Mater.*, 2000, **48**, 4501–4515.
104. Qian, H. and Luo, J., Vanadia-based equilibrium-thickness amorphous films on anatase (1 0 1) surfaces. *Appl. Phys. Lett.*, 2007, **91**, 061909, 3 pp.
105. Qian, H., Luo, J. and Chiang, Y.-M., Anisotropic wetting of ZnO by Bi_2O_3 with and without nanometer-thick surficial amorphous films. *Acta Mater.*, 2008, **56**, 862–873.
106. Izaki, M., Electrochemical preparation of transparent ferromagnetic Fe–Zn–O heterogranular films. In *Moscow International Symposium on Magnetism*, ed. N. Perov *et al.* Lomonosov State University, Moscow, 2008, p. 703.